Atomic delay in helium, neon, argon and krypton

2014 J. Phys. B: At. Mol. Opt. Phys. 47 245003

(http://iopscience.iop.org/0953-4075/47/24/245003)

IOP Publishing Journal of Physics B: Atomic, Molecular and Optical Physics

J. Phys. B: At. Mol. Opt. Phys. **47** (2014) 245003 (7pp) doi:10.1088/0953-4075/47/24/245003

Atomic delay in helium, neon, argon and krypton*

Caryn Palatchi[1], J M Dahlström[2,3,4], A S Kheifets[5], I A Ivanov[5], D M Canaday[1], P Agostini[1] and L F DiMauro[1]

[1] The Ohio State University, Department of Physics, Columbus, OH 43210, USA
[2] Department of Physics, Stockholm University, AlbaNova University Center, SE-10691 Stockholm, Sweden
[3] Max Planck Institute for the Physics of Complex Systems, Noethnitzer Str. 38, D-01187 Dresden, Germany
[4] Center for Free-Electron Laser Science, Luruper Chaussee 149, D-22761 Hamburg, Germany
[5] Research School of Physics and Engineering, The Australian National University, Canberra ACT 0200, Australia

E-mail: palatchi.1@buckeyemail.osu.edu

Received 11 June 2014, revised 4 October 2014
Accepted for publication 10 October 2014
Published 3 December 2014

Abstract

Photoionization by an eXtreme UltraViolet (XUV) attosecond pulse train (APT) in the presence of an infrared pulse (RABBITT method) conveys information about the atomic photoionization delay. By taking the difference of the spectral delays between pairs of rare gases (Ar,He), (Kr, He) and (Ne,He) it is possible to eliminate in each case the larger group delay ('attochirp') associated with the APT itself and obtain the Ar, Kr and Ne Wigner delays referenced to model calculations of the He delay. In this work we measure how the delays vary as a function of XUV photon energy but we cannot determine the absolute delay difference between atoms due to lack of precise knowledge of the initial conditions. The extracted delays are compared with several theoretical predictions and the results are consistent within 30 as over the energy range from 10 to 50 eV. An 'effective' Wigner delay over all emission angles is found to be more consistent with our angle-integrated measurement near the Cooper minimum in Ar. We observe a few irregular features in the delay that may be signatures of resonances.

Keywords: attosecond, delay, photoionization

(Some figures may appear in colour only in the online journal)

1. Introduction

Atomic photoionization is the process by which an electron in a bound atomic state absorbs a photon and makes a transition to a continuum state in which there is a finite probability to detect the electron at macroscopic distances from the nucleus. Photoionization can be regarded as a quantum jump, which occurs instantaneously at any moment in the field, but in the case of coherent ionizing fields it is often more meaningful to consider the process in the time-dependent wave packet picture. While there is no such thing as a time operator in quantum mechanics, the delay in photoionization can be a quantum dynamical observable [1–5] when it is understood as a temporal delay in the departure of the outgoing electron wave packet relative to the arrival of the XUV pulse[6].

Photoionization by a combined eXtreme UltraViolet (XUV) field and an infrared (IR) field is the basic scheme used in attosecond science for characterization of both single attosecond pulses (SAPs) and attosecond pulse trains (APT). For SAP, the attosecond streak-camera method [6] is used to monitor the final momentum of the photoelectron as a function of the phase between the IR laser and the SAP. The temporal structure of the SAP can then be determined by comparison with numerical simulations [7]. In contrast, an

* Intended contribution to the 'Special issue on ultrafast electron and molecular dynamics' available at http://iopscience.iop.org/0953-4075/47/12.

[6] Smith [3] introduces the lifetime matrix **Q** in collision theory. When **Q** is diagonalized, its eigenvalues are the lifetimes of metastable states.

APT corresponds to odd harmonics in the frequency domain and the reconstruction of attosecond beating by interference of two-photon transitions (RABBITT) method [8] utilizes sidebands in the photoelectron energy spectrum that arise due to interference of degenerate quantum paths into the continuum. In the perturbative regime, the intensity of these weak sidebands modulate like cosine functions over the delay between IR laser and APT and their relative phases can be used to characterize the average temporal structure of the attosecond pulses in the train [9].

While none of these methods, strictly speaking, provide an absolute photoionization delay, observing the simultaneous photoemission from different atomic orbitals has revealed a differential delay. Streaking measurements of the photoelectrons promoted from the 2s and 2p orbitals in neon by a SAP resulted in a relative delay of 21 as, about twice larger than that predicted by theory [10–14]. This measurement stimulated further theoretical work which addressed the accuracy of attosecond streaking measurements and lead to the conclusion that part of the observed delay in streaking is due to a coupling of the long-range Coulomb potential and the IR field [4, 13, 15–19]. In other studies, based on RABBITT, APTs have been used to determine a delay of ∼100 as between the 3p and 3s orbitals of argon [20, 21]. In this case, the observed delay can be readily understood as a difference in 'atomic delay' between the two orbitals which is directly related to phase differences of two-photon matrix elements. Although the concept of delay in RABBITT measurements is not as intuitive as in streaking, theoretical calculations show that both schemes are closely related [4, 5, 16].

Various theoretical approaches have been used to model the experiments: multielectron screening effects due to electron correlation have been accounted for using random-phase approximation with exchange (RPAE) for absorption of a single XUV photon [12, 22] and for the two-color (XUV+IR) case [13, 23]. Other approaches for correlation include the state-specific expansion approach [10], the time-dependent R-matrix [11], two-electron models [24] and a multi-configuration Hartree–Fock (MCHF) close-coupling ansatz [25], time-dependent local density approximation (TDLDA) [26] and *B*-spline R-matrix (BSRM) calculations [14]. As already mentioned, only a fraction of the experimentally measured neon subshell delay has been accounted for [10–14]. The experimentally measured argon subshell delay [20, 21] is in reasonable agreement with the MCHF [25] and TDLDA calculations [26]. Prior to these correlated calculations, there has also been modeling of the atomic delay for various noble gas atoms by single-active electron, time-dependent simulations [27].

It has been suggested that more delay measurements are needed in energy regions where inter-shell correlation effects are marginal and where various models can be more easily tested [4]. In this paper, we compare RABBITT measurements with various calculations in an attempt to shed some additional light on the topic of atomic delay and its relation to the Wigner delay in photoionization. The experiments are performed on various inert gas atoms over a broader energy range than previous reports. In principle, an ideal experiment would expose a gas mixture to the same APT but this is not practical for technical reasons. Alternately, we use a differential method by conducting successive RABBITT measurements on different target gases for *nearly* identical APT. Under these conditions, the high harmonic group delay dispersion (GDD) from different gases can be assumed to be the same and thus cancels out. As we successively perform RABBITT measurements in different targets atoms, the exact initial condition can not be reproduced for the delay between the APT and IR laser. As a consequence, we are not able to determine the absolute delay difference between the targets but we are able to monitor variation of the delay difference as a function of XUV photon energy. In our experiment helium atom is choosen as a reference target.

2. Method

A RABBITT measurement probes the frequency response function of an atomic system in the process of photoionization by an XUV field and an additional phase-locked reference IR laser field. The APT is synthesized from a comb of odd-order high harmonics generated by a suitable high-density gas upstream of the RABBITT measurement. In the current study, neon is used as the APT generator gas. The APT propagates into the RABBITT chamber and we observe strong photoelectron peaks corresponding to one-photon absorption of the XUV harmonics and weaker sideband peaks that originate from XUV-IR two-photon processes. The electron wave packet is thus measured in the frequency domain (photoelectron energy), but additional information about the timing is gained by repeating the experiment for all delays between the APT and IR laser.

The delay measured by the RABBITT method has contributions from both the generation and target gas. The largest contribution is typically due to the GDD of the APT (or 'attochirp') which is the second spectral derivative of the harmonic phase [28]. The attochirp defines the main time structure of the attosecond pulses, but the pulses also contains smaller contributions from the generating atom itself, this term is usually the quantity of interest in high-harmonic spectroscopy [29, 30]. In addition, the target atom introduces a delay due to the two-photon transitions of the RABBITT scheme that we call the *atomic delay*, τ_θ. This delay can be decomposed as a Wigner-like delay τ_W that describes the delay of the electron in photoionization and a continuum–continuum delay τ_{cc} that arises due to the motion of the electron in the combined IR and ionic field [4] (also called Coulomb–laser coupling in the context of streaking, see [5, 15, 16]). In a differential measurement the delay of the generator cancels out and access to the differential atomic delay can be obtained, see [21].

To calibrate the measurement, we use the simplest system at our disposal, the helium atom, and then compare this RABBITT measurement with that of more complex systems: neon, argon and krypton atoms. It is important to understand in assessing delay in photoionization that the 'delay' corresponds to a quantum mechanical phase and that only differences can be measured, hence any experiment of this kind must be comparative. For example, the experiments by Guenot *et al* [20] and Schultze *et al* [10] make an intra-

species comparisons between subshells of a given atom while here we present an inter-species measurement. There are certain factors distinguishing these two approaches. In intra-species comparisons, the measurement is performed on both subshells simultaneously and in order to avoid degeneracy in the photoelectron energy, the range of the measurement must be restricted. However, the present measurement is distinct since it attempts to assess a different quantity. Here the dependence of the atomic delay as a function of energy is evaluated, rather than the absolute temporal difference between photoionization processes of separate subshells at a specific energy.

2.1. RABBITT measurement

The RABBITT method is an interferometric technique typically used to characterize the temporal profile of XUV APT. An intense IR pulse with frequency ω_f is split into two portions: the pump and the probe. The pump is used to drive the HHG process, producing the APT with anti-periodicity of $1/2\,\omega_f$ (with alternating sign of the XUV field between adjacent half-cycles of the IR field). The XUV spectral content is then measured downstream of the source using a photoelectron energy spectrometer (PES). The phase-locked probe is recombined with the XUV APT such that temporal and spatial overlap is established in the detection gas of the PES. The IR probe perturbs the single-photon ionization process, driving two-photon ionization and producing photoelectrons with energies corresponding to even-order harmonics called sidebands. As the probe delay is scanned relative to the APT, the sideband amplitudes will oscillate due to the quantum interference between the two degenerate paths into the continuum. The relative phase of the sideband oscillations versus energy gives the derivative of the spectral phase. Thus, RABBITT measures both the spectral magnitude and the spectral phase.

The RABBITT experiment presented here was conducted using a 60 fs, 0.78 μm beam with 250 μJ pulse energy and operating at a 1 kHz repetition rate. The s-polarized pulse is expanded with a 2X telescope and split into two beams using a 50/50 beamsplitter. The transmitted pump pulse, focused with a 20 cm lens, generates high harmonics in a Ne gas jet produced with a 0.25 mm diameter nozzle backed with $\leqslant 0.3$ bar. We estimate an intensity of 9×10^{14} W cm^{-2} at the gas jet position based on our focusing geometry and a 1.2 mm Rayleigh range. Due to the tight focal conditions and free jet expansion, the gas density is spread across the Rayleigh range which means the gas is exposed to a range of intensities lower than calculated geometrically; hence the observed neon harmonic cutoff is 100–120 eV.

The IR pump and high harmonics are respectively absorbed by and transmitted through a 0.2 μm thick Al filter. The reflected probe pulse was delayed with a set of piezo-controlled wedges and recombined with the harmonic beam using a silver mirror with 1 cm diameter aperture, allowing for an acceptance angle of 2.5 mrad off-axis for the harmonics. A gold toroidal mirror was used to refocus the harmonics and probe beam into our detection apparatus: a magnetic bottle time-of-flight electron spectrometer [31]. A 5 V dc-potential is applied to the spectrometer flight tube at the midway point (0.55 m) to facilitate collection of the lower energy electrons ($\leqslant$5 V). Conversely, we have found no effect on the RABBITT group delay as the potential is systematically varied over the range of 0–30 eV. He, Ne, Ar and Kr detection gases were used with backing pressures of 280 torr, 460 torr, 390 torr and 520 torr, respectively. Space charge effects are negligible due to the small number of electrons generated per shot which is at maximum 30 in a cube of 100 μm on each side [32].

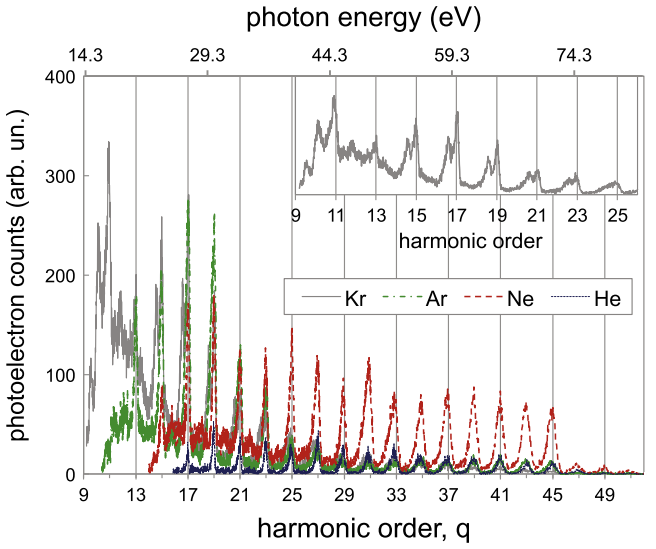

Figure 1. The angle-integrated electron energy distribution versus harmonic order, q, (bottom axis) and photon energy (top axis) for various inert gas atoms ionized by a harmonic comb generated in a neon source pumped by an intense 0.78 μm pulse. The RABBITT detection gases are krypton (grey line), argon (green dashed–dotted line), neon (red dashed line) and helium (blue dotted line).

2.2. Results

RABBITT scans were taken by accumulating 1–1.5 $\times$ 10^4 laser shots at each probe delay. The probe delay was scanned in 70 steps of 0.2 fs producing 10.6 sideband oscillation cycles at twice the fundamental frequency. Scans for each detection gas were performed one after the other, without changing harmonic generation conditions. Helium was used as the common reference gas. The accumulated photoelectron spectra from harmonics generated in Ne, passing through an Al filter and detected in He, Ne, Ar, and Kr are shown in figure 1. The high harmonic comb is visible up to the Aluminum filter transmission cutoff at 70 eV (harmonic order 45). The variation in amplitude between the various spectra reflects both the photoionization cross-section of each detection gas and the backing pressure used. Additionally, unlike the other noble gases, Kr has a large enough fine structure splitting (0.665 eV) to be resolvable in the photoelectron energy spectra (see inset figure 1). The harmonics and sidebands from both the krypton $^2P_{1/2}$ and the $^2P_{3/2}$ channels are independently monitored in the PES.

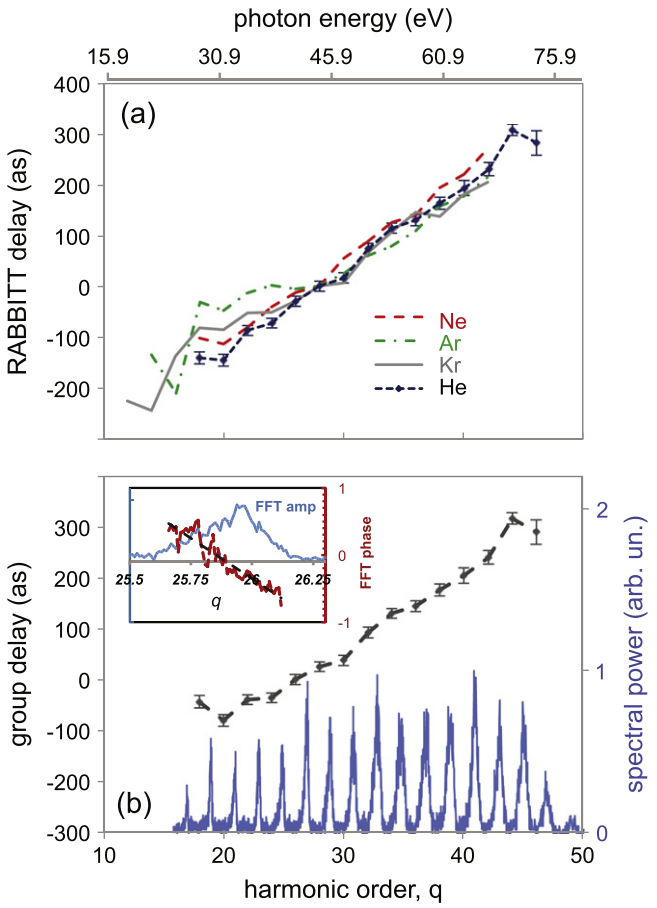

Figure 2. (a) The RABBITT delay versus harmonic order, q, (bottom axis) and photon energy (top axis) detected in various target inert gases. (b) Attosecond pulse train group delay (dash line) and spectrum (solid line) generated in neon and detected in helium (reference) target. Note, the comb amplitude decreases at the Al-filter absorption edge (~70 eV). The inset is a plot of the FFT amplitude (blue line) and phase (red dashed line) of the 26-order harmonic sideband detected in helium, see text for discussion.

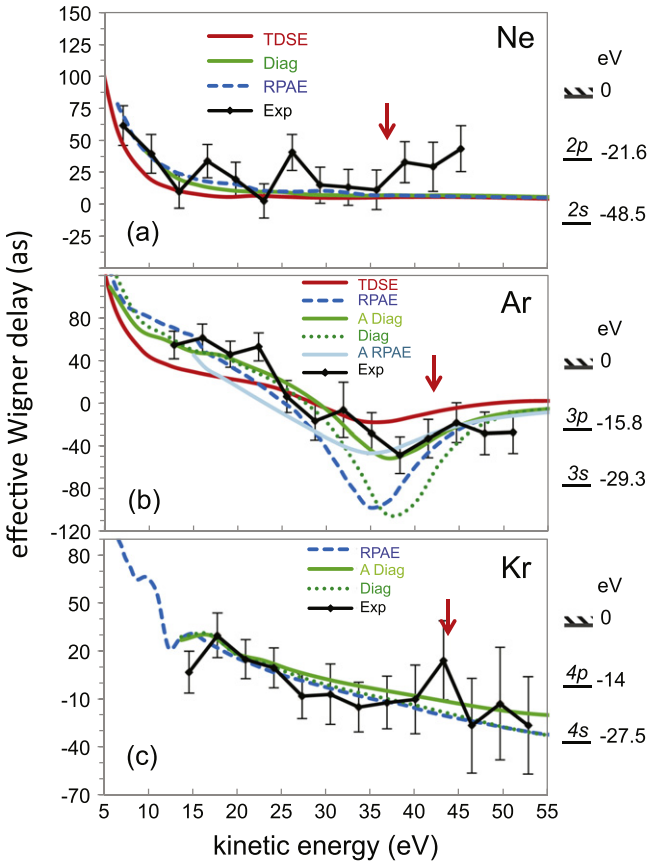

Figure 3. Comparison of the effective Wigner delay from experiment and theory for (a) neon, (b) argon and (c) krypton versus photoelectron kinetic energy, E_e. The photon energy is simply given as $E_p = E_e + I_p$, where I_p is the ionization potential and is 21.6 (Ne), 15.8 eV (Ar) and 14 eV (Kr) [40]. The TDSE-SAE calculation is from [27], Diag ≡ diagrammatic calculations from [13], 'RPAE' from [22] and Exp ≡ experiment. The calculations labelled with a 'A' in the legend are angle-integrated. The red arrow in each marks the start of the region of helium doubly excited states, see text for discussion. The valence subshell energy levels are shown for each gas on the right hand side.

The results of the RABBITT scans are displayed in figure 2(a). The quantity measured by the RABBITT technique is $\tau_{\mathrm{RABBITT}} = \tau_{\mathrm{GD}} + \tau_\theta$, where τ_{GD} corresponds to the group delay of the attosecond pulse and where τ_θ is the atomic delay of the target. To extract the RABBITT phase from the He, Ne and Ar target scans, we use a least-squares method in which each sideband is integrated within a window defined as $0.2E_f$ (E_f is the fundamental photon energy, 1.6 eV) and fit to a Cosine function where the phase is a fit parameter and the error bars are the standard deviation. For the special case of Kr in which the fine-structure is resolvable, we extract the RABBITT phase using a narrow $0.15E_f$ window centered on the sidebands from the $^2P_{3/2}$ state only. The Kr RABBITT results for $j = 3/2$ are shown in figure 2(a). There are multiple contributions that are reflected in our error bars including short term intensity fluctuations, chirp across sidebands and interferometric instability.

In order to gain some insight into the uncertainty in an individual sideband's phase value, e.g. error bars, we also perform a FFT analysis. As an example, the inset in figure 2(b) displays the FFT magnitude (blue line) and phase (dashed red line) at frequency $2\omega_f$ across the 26-order sideband of a He RABBITT scan. For this case, a phase variation (chirp) of ~ -1 rad eV^{-1} (0.4 fs eV^{-1}) is observed. We find that this sideband chirp can vary for different orders and on different days. Note, we find that any variations in phase over the duration of the data run is small in comparison, e.g. typically less than 0.1 radians over 3 hr. This phase variation is an error inherent in these measurements, which were taken in succession in approximately 15 min intervals, and can be understood by the fact that the harmonic pulse train is finite. The phase variation contributes to our final error since the phase is extracted from a measurement that has contributions from the bandwidths of the harmonic and the dressing fields, and the finite resolution of our electron energy spectrometer (~0.5%). As illustrated in the inset in figure 2(b), the weighted chirp contributes over the full-width half maximum of the sideband amplitude in the frequency domain. Equivalently, the chirp can be thought as an error in the argument of

the Cosine function in the time domain analysis described above. Our error bars in figures 2 and 3 represent this systematic error, as well as statistical fluctuations. Furthermore, our studies show that phase retrieval using either the time or frequency domain method results in consistent values. It should be emphasized that the RABBITT measurement is only sensitive to the phase difference $\Delta\phi_q = 2\omega_f\tau_q$ between consecutive harmonics of order $(q+1)$ and $(q-1)$ and that it is, therefore, insensitive to absolute phase of the XUV harmonics. Further, our measurement is conducted without absolute knowledge of the delay between the APT and IR field, which leads to an unknown constant shift in delay of the RABBITT scans. Theoretical calculations [13, 22, 27] show that the atomic delays for He, Ne, Ar and Kr are approximately equal (within 10 as) at a photon energy of ~45 eV, so we shift our raw data to overlap at the 28-order sideband (44.5 eV photon energy).

Figure 2(b) shows the extracted group delay and the APT spectrum from the neon high harmonic source and helium detector. The APT spectrum is determined by dividing the measured spectrum by the photoionization cross-section of the helium detection gas [33]. The APT group delay (up to an unknown overall constant) is extracted via $\tau_{GD} = \tau_{RABBITT,He} - \tau_{\theta,He}$, where $\tau_{RABBITT,He}$ is the measured RABBITT delay with He detection gas and $\tau_{\theta,He}$ is the He delay calculated by Mauritsson *et al* [27] using numerical solutions of the time-dependent Schrödinger equation within the single-active electron approximation[7]. We observe that the harmonic group delay has a positive dispersion in this measurement, indicative of phase-matched short trajectories. The APT group delays together with the continuum–continuum delays are used to extract an effective Wigner delay from the experimental data for Ne, Ar and Kr via $\tau_W = \tau_{RABBITT} - \tau_{GD} - \tau_{cc}$ (up to an unknown overall constant). Here we write 'effective' because the measurement is done over integrated emission angles and not uniquely along the polarization axis of the fields. The results of our extraction of Ne, Ar, and Kr atomic delays are displayed in figure 3. We note that it is not strictly necessary to rely on the theoretically calculated Helium atomic delay to analyze these data, we could simply show $\tau_{RABBITT,Kr} - \tau_{RABBITT,He} + \tau_0$, where τ_0 is an unknown constant due to the lack of interferometer stability between the two measurements, in direct comparison with the theoretical atomic delays, $\tau_{\theta,Kr} - \tau_{\theta,He}$. However, the one-photon ionization delay for an individual atom is of more interest as a quantity and we, therefore, show the effective Wigner delay, $\tau_W + \tau_0$, for Ne, Ar, and Kr in figure 3[8].

[7] We have verified that this model for He differs by less that 2 as as compared to an exact two-electron calculations by Ivanov at the reference photon energy of 45 eV. However, artefact contributions from helium resonances may be present in our extracted delays at higher XUV photon energies.

[8] If the reader prefers to examine the inter-species delay differences explicitly, the raw data are provided in figure 2 for that purpose.

3. Discussion

We compare our results with calculations by Mauritsson *et al* [27], Dahlström *et al* [13] and Kheifets [22]. Mauritsson *et al* employs a nonperturbative, time-dependent method within the single-active-electron approximation to calculate the angle-integrated atomic delays of He, Ne, and Ar. Dahlström uses time-independent formalism based on diagrammatic many-body perturbation theory to calculate the atomic delay in Ne and Ar. We also perform additional diagrammatic calculations for Kr. The diagrammatic calculations are performed for two cases: the angle-resolved case [13] in which the photoelectron is ejected along the polarization axis of the field and the newly calculated angle-integrated case. To obtain the Wigner delays from the time-dependent calculations by Mauritsson and from the two-photon diagrammatic calculations by Dahlström, we subtract the universal continuum–continuum delay calculated for hydrogen at 0.8 μm [4]. In contrast, both angle-resolved and effective (angle-averaged) Wigner delays are computed directly by the one-photon RPAE method by Kheifets. The RPAE and the diagrammatic method both account for inter-shell screening effects of the XUV photon in ionization of Ne, Ar and Kr.

The experimentally extracted photoionization delay of Ne is shown in figure 3(a). Note that all experimental delay curves in figure 3 are shifted by a constant value to best match the theoretical data. The simulation by Mauritsson, the diagrammatic calculation and the RPAE calculation yield very similar results in neon and agrees with our measurement to within ~30 as. Interestingly, our data contains some irregular structures that could be a result of resonances not included in the theoretical calculations. Such resonances were included in the BSRM calculation [14]. However, they reported the time delay results at a much higher photon energy range not covered by the present study.

The experimentally measured photoionization delay of Ar is compared with various calculations in figure 3(b). When comparing with theory, we emphasize that only the overall structure of the delay curve with respect to energy is physically relevant quantity. We find the recent angle-integrated diagrammatic and RPAE calculations most closely reproduces the overall structure of our experimental results. However, the experimental results deviate from the angle-resolved diagrammatic and RPAE calculations in the region near the Cooper minimum of Argon [34], where two angular channels contribute in photoionization. Note, the influence of the Cooper minimum in the high harmonic recombination dipole was recently reported [35] in an angle-resolved measurement and shows good agreement with the larger phase variation predicted by our angle-resolved calculations in figure 3(b). However, our 2π-magnetic bottle spectrometer results in an angle-integrated measurement which reduces the apparent delay and is also verified by our calculations. This implies that our measured delay is not the Wigner delay along the polarization axis of the fields but rather an 'effective' delay over all emission angles. Also, our data shows additional irregular features that could be an experimental signature of resonances in the target ion, as predicted theoretically by

Carette *et al* [25]. A deeper understanding of how these resonances affect the attosecond time delay experiments may prove essential for future attosecond experiments.

It has been shown experimentally that resonances in the both molecular and atomic systems can give rise to irregular structures in the RABBITT scans [37, 38]. The resonances will lead to shifts of the sideband modulations that depends on the detuning of the XUV harmonic, the lifetime of the resonance and the bandwidth of the harmonics. Since the IR photon is much larger than the typical structure of the auto-ionizing resonance, the Wigner delay can no longer be obtained using the RABBITT method in the usual sense. Large structures due to resonances in argon has been predicted using the MCHF method that includes double excited states [25]. Interestingly, time-dependent simulations of two-color (XUV–IR) ionization of N_2 has revealed that these shifts can be related to the photoelectron release time if the field frequencies can be tuned [39], but such measurements are not presented in the current work. Instead, we speculate on possible structures in the experimental measurements that can be due to resonances: first, we point out that autoionizing resonances occur at ~58 eV for helium (our reference system). The deviations from the theory that occurs at the high photon energy range ~58 eV (37 eV kinetic energy in figure 3 (a)) for neon are likely signatures from the helium resonances that are not included in the single-active electron reference calculations by Mauritsson *et al* [27]. Similarly, irregular features around this photon energy are expected in argon and krypton (red arrows). In figure 3(a) the neon data exhibits a peak structure at XUV photon energies corresponding to the Rydberg series that leads to the opening of the 2s ionization channel: 45.6–48.5 eV (24–27 eV kinetic energy) [40]. In figure 3(b) the argon data also shows some weak structure in the XUV range between 35–40 eV (9–14 eV kinetic energy) which we attribute to double excited states where two 3p) electrons are excited, which lead to the $3s^2 3p^4 nl$-thresholds [41]. The importance of such resonances has been discussed by Carette *et al* [25]. Further structures at XUV energy close to 49 eV (23 eV kinetic energy) occur due to argon states that have double excitation from both the 3p and 3s, e.g. the $3s^1 3p^5 4p^2$ configuration, as was confirmed using the Los Alamos atomic physics codes [43].

One other possible source of disagreement between experiment and theory that must be considered is the contribution of sub-shell valence ionization. In Ar, the 3s state (binding energy of 29.3 eV [44]) leads to the appearance of harmonic peaks at shifted photoelectron energies with respect to the 3p channel. For the 0.78 μm fundamental driver, the 3s and 3p peaks are separated by ~0.75 eV. We can estimate the 3s subshell contributions from knowledge of the photo-ionization cross-sections, Al filter transmission function, 3s and 3p peak separation, observed peak widths and the integration window used in our analysis. Based on this analysis we estimate that the 3s channel is over two orders of magnitude smaller than the contribution from the 3p, even in the vicinity of the Cooper minimum [34]. Hence, any 3s contributions to our argon RABBITT measurement can be neglected.

Figure 3(c) shows the effective Wigner delay of Kr. Both the RPAE calculation [22] and the angle-integrated diagrammatic calculation show a small peak near 15 eV kinetic energy, the measurement also shows a similar deviation. At higher energy, the experiment displays another structure near 43 eV kinetic energy that deviate from the calculations. As discussed earlier, the helium doubly excited states, absent in our reference atom calculation is one potential cause of this deviation. However, it is also possible that photoionization from the Kr 4s valence subshell could also contribute. In the kinetic energy spectrum, the 4s photoelectron peak is expected to occur at approximately 0.7 eV ($j = 3/2$) and 0.1 eV ($j = 1/2$) from the 4p valence level [40]. Thus, we have restricted our analysis to a narrow energy window centered on the $j = 3/2$ peaks only. As long as the fine-structure is resolvable, the contributions from the 4s channel are kept minimal: one to two orders of magnitude smaller than the 4p. However, the spectrometer's resolution decreases with increasing kinetic energy and at 40 eV the harmonic width becomes comparable to the Kr fine-structure splitting and no longer resolvable. For data points near 40 eV kinetic energy, we estimate that the 4s/4p ratio can vary from 1/12 to 1/3 depending upon the placement of our energy window. Above 44 eV kinetic energy the 4s contribution is again negligible since the Al filter absorption edge suppresses any photons above 70 eV thus closing the 4s channel.

The stability of the attochirp is crucial for our experimental results. A consequence of the attochirp is that target atom encounters the lower frequency components of the APT, thus effectively photoionizing before the arrival of the higher frequencies. In the time domain, we are using a train of ~200 as pulses to probe a process which occurs on a timescale an order of magnitude smaller. Furthermore, our error bars are on the order of the photoionzation delay in some cases. We emphasis that the measurement is only possible because the driver is not an isolated attosecond pulse but rather a pulse train which makes the harmonic peaks distinct and well-defined in energy. The process of photoionization may be close to instantaneous but not so rapid as to be immeasurable, as demonstarted by our experiments ability to reveal a variation of the atomic delay as a function of XUV photon energy by difference of various inert gas atoms.

In conclusion, an APT produced by a neon high harmonic source was used to measure the variation of atomic delay with photon energy for Ne, Ar and Kr relative to the He using the RABBITT method. Our data covers a wide energy range but lacks information about the absolute delay difference due the nature of our experimental method. The extracted atomic delays were compared with several theories over a large energy range (10–50 eV) and found to be consistency to within ~30 as. Angle-integrated calculations are found to be more consistent with our measurement near the argon Cooper minimum than angle-resolved calculations. We observed a few irregular features in the delay that we suspect are due to resonances.

Note added in proof: it has come to our attention that independent experimental investigations have been conducted using different methodological approaches that allow for absolute determination of the delay difference by either: (i) active stabilization of the interferometer [36, 45] or by (ii) coincidence detection from a mixed target gas [46]. The detailed role of resonances in RABBITT for Helium are discussed in [47].

Acknowledgments

The work at The Ohio State University was supported under DOE contract DE-FG02-04ER15614. LFD acknowledges support from the OSU Hagenlocker chair. DMC acknowledges support from the NSF REU contract PHY-1304218. JMD acknowledges support from the Swedish Research Council (VR). ASK acknowledges support by the Australian Research Council in the form of the Discovery grant DP120101805. The authors like to thank Dietrich Kiesewetter for assistance.

References

[1] Eisenbud L 1948 *PhD Thesis* Princeton University
[2] Wigner E P 1955 *Phys. Rev.* **98** 145
[3] Smith F T 1960 *Phys. Rev.* **118** 349
[4] Dahlström J M, LHuillier A and Maquet A 2012 *J. Phys. B: At. Mol. Opt. Phys.* **45** 183001
[5] Pazourek R, Nagele S and Burgdörfer J 2013 *Faraday Discuss.* **163** 353
[6] Itatani J, Quéré F, Yudin G L, Yu Ivanov M, Krausz F and Corkum P B 2002 *Phys. Rev. Lett.* **88** 173903
[7] Mairesse Y and Quéré F 2005 *Phys. Rev.* A **71** 011401
[8] Muller H G 2002 *Appl. Phys.* B **74** S17
[9] Véniard V, Taïeb R and Maquet A 1996 *Phys. Rev.* A **54** 721
[10] Schultze M *et al* 2010 *Science* **328** 1658
[11] Moore L R, Lysaght M A, Parker J S, van der Hart H W and Taylor K T 2011 *Phys. Rev.* A **84** 061404
[12] Kheifets A S and Ivanov I A 2010 *Phys. Rev. Lett.* **105** 233002
[13] Dahlström J M, Carette T and Lindroth E 2012 *Phys. Rev.* A **86** 061402
[14] Feist J, Zatsarinny O, Nagele S, Pazourek R, Burgdörfer J, Guan X, Bartschat K and Schneider B I 2014 *Phys. Rev.* A **89** 033417
[15] Ivanov M and Smirnova O 2011 *Phys. Rev. Lett.* **107** 213605
[16] Zhang C H and Thumm U 2010 *Phys. Rev.* A **82** 043405
[17] Zhang C H and Thumm U 2011 *Phys. Rev.* A **84** 033401
[18] Nagele S, Pazourek R, Feist J, Doblhoff-Dier K, Lemell C, Tòkèsi K and Burgdörfer J 2011 *J. Phys. B: At. Mol. Opt. Phys.* **4** 081001
[19] Dahlström J M, Guènot D, Klünder K, Gisselbrecht M, Mauritsson J, LHuillier A, Maquet A and Taïebs R 2013 *Chem. Phys.* **414** 53
[20] Guénot D *et al* 2012 *Phys. Rev.* A **85** 053424
[21] Klünder K *et al* 2011 *Phys. Rev. Lett.* **106** 143002
[22] Kheifets A S 2013 *Phys. Rev.* A **87** 063404
[23] Dahlström J M and Lindroth E 2014 *J. Phys. B: At. Mol. Opt. Phys.* **47** 124012
[24] Nagele S, Pazourek R, Feist J and Burgdörfer J 2012 *Phys. Rev.* A **85** 033401
[25] Carette T, Dahlström J M, Argenti L and Lindroth E 2013 *Phys. Rev.* A **87** 023420
[26] Dixit G, Chakraborty H S and Madjet M 2013 *Phys. Rev. Lett.* **111** 203003
[27] Mauritsson J, Gaarde M B and Schafer K J 2005 *Phys. Rev.* A **72** 013401
[28] Mairesse Y *et al* 2003 *Science* **302** 1540
[29] Shafir D, Soifer H, Bruner B D, Dagan M, Mairesse Y, Patchkovskii S, Yu Ivanov M, Smirnova O and Dudovich N 2012 *Nature* **485** 343
[30] Kraus P M, Rupenyan A and Worner H J 2012 *Phys. Rev. Lett.* **109** 233903
[31] Roedig C A 2012 *PhD Thesis* The Ohio State University (https://etd.ohiolink.edu/ap/10?9555268531310::NO:10:P10_ETD_SUBID:76210)
[32] Chirla R C 2011 *PhD Thesis* The Ohio State University (https://etd.ohiolink.edu/ap/10?9555268531310::NO:10:P10_ETD_SUBID:74824)
[33] Samson J A R and Stolte W C 2002 *J. Electron. Spectrosc. Relat. Phenom.* **123** 265
[34] Cooper J W 1962 *Phys. Rev.* **128** 681
[35] Schoun S B, Chirla R, Wheeler J, Roedig C, Agostini P, DiMauro L F, Schafer K J and Gaarde M B 2014 *Phys. Rev. Lett.* **112** 153001
[36] Guénot D 2014 *J. Phys. B: At. Mol. Opt. Phys.* **47** 245602
[37] Haessler S *et al* 2009 *Phys. Rev.* A **80** 011404(R)
[38] Swoboda M *et al* 2010 *Phys. Rev. Lett.* **104** 103003
[39] Caillat J *et al* 2011 *Phys. Rev. Lett.* **106** 093002
[40] Ralchenko Y, Kramida A E, Reader J and NIST ASD Team, 2011 *NIST Atomic Spectra Database* (version 3.1.5) (National Institute of Standards and Technology, Gaithersburg, MD) (http://physics.nist.gov/asd)
[41] van der Hart H W and Greene C H 1998 *Phys. Rev.* A **58** 2097
[42] Minnhagen L 1963 *Ark. Fys.* **25** 203
[43] Cowan R D 1981 *Theory of Atomic Spectra* (Berkely, CA: University of California Press) (http://aphysics2.lanl.gov/tempweb/lanl/)
[44] CRC *Handbook of Chemistry and Physics* 92nd edn
[45] Guénot D 2014 *PhD Thesis* Lund University
[46] Sabbar M, Heuser S, Boge R, Lucchini M, Gallmann L, Cirelli C and Keller U 2014 arXiv:1407.6623
[47] Jimenez-Galán Á, Argenti L and Martín F 2014 arXiv:1405.4732v1